

PCCP

Accepted Manuscript



This is an *Accepted Manuscript*, which has been through the Royal Society of Chemistry peer review process and has been accepted for publication.

Accepted Manuscripts are published online shortly after acceptance, before technical editing, formatting and proof reading. Using this free service, authors can make their results available to the community, in citable form, before we publish the edited article. We will replace this *Accepted Manuscript* with the edited and formatted *Advance Article* as soon as it is available.

You can find more information about *Accepted Manuscripts* in the [Information for Authors](#).

Please note that technical editing may introduce minor changes to the text and/or graphics, which may alter content. The journal's standard [Terms & Conditions](#) and the [Ethical guidelines](#) still apply. In no event shall the Royal Society of Chemistry be held responsible for any errors or omissions in this *Accepted Manuscript* or any consequences arising from the use of any information it contains.



PCCP

PAPER

A Soluble Cryogenic Thermometer with High Sensitivity based on Excited-state Configuration Transformations

Jianwei Chen^{a,b}, Yishi Wu^{a,*}, Xuedong Wang^{a,b}, Zhenyi Yu^{a,b}, He Tian^{d,*}, Jiannian Yao^{a,*}, Hongbing Fu^{a,c,*}

Received 00th January 20xx,
Accepted 00th January 20xx

DOI: 10.1039/x0xx00000x

www.rsc.org/

Cryogenic temperature detection plays an irreplaceable role in the exploring of the nature. Developing high sensitivity, accurate, observable and convenient measurements of cryogenic temperature is not only a challenge but also an opportunity for the thermometer field. The small molecule 9-(9,9-dimethyl-9H-fluoren-3yl)-14-phenyl-9,14-dihydrodibenzo[a,c]phenazine (FIPAC) in 2-methyl-tetrahydrofuran (MeTHF) solution is utilized for the detection of cryogenic temperature with a wide range from 138 K to 343 K. This system possesses significantly high sensitivity at low temperature, which reaches as high as 19.4 % per K at 138 K. The temperature-dependent ratio of the dual emission intensity can be fitted as a single-exponential curve as the function of temperature. This single-exponential curve can be explained by the mechanism that the dual emission feature of FIPAC results from the excited-state configuration transformations upon heating or cooling, which is far more different from the previously reported mechanisms. Here, our work gives an overall interpretation for this mechanism. Therefore, application of FIPAC as cryogenic thermometer is experimental and theoretical feasible.

Introduction

Temperature is probably one of the most frequently measured physics parameters in the exploring of the nature. Among the range of techniques for the measurement of temperature, luminescent temperature sensors have been the observable of choice due to the advantages of noninvasive, observability, high sensitivity and large-scale imaging.¹⁻⁸ To date, small organic molecules, metal-ligand complexes, lanthanide complexes, polymers and nanoparticles have been operated both in the liquid or solid phase on the temperature-dependent optical signals including wavelength, lifetime, intensity and anisotropy.⁹⁻¹⁷ In addition, soluble luminescence-dependent systems applied in temperature sensor make the detection of temperature spatially resolved, which gives a more precise temperature data.¹⁸ Recently, dual emission systems receive considerable interest.^{1, 5, 13, 18-25} Different systems have various mechanisms for the feature of dual emission, such as charge-transfer state,^{19, 20} excimer of molecules,²¹ hybridize quantum dots,²² tautomer excited state intramolecular proton transfer,²⁴ and clusters interactions.²⁵ For the temperature-dependent ratio of the dual emission intensity, many dual emission systems are applied in thermometer field.^{13, 18, 24, 25} The range in the ratio of the dual

emission intensity demonstrates a temperature-dependent PL color map, which can be taken as a parameter for the detection of temperature.

On the other hand, with the developing of space exploration, material research and dipolar adventure, cryogenic temperature detection will undoubtedly play an irreplaceable role in the thermometer field.²⁶ Therefore, high sensitivity, accurate, observable, and convenient measurement of cryogenic temperature is an impending task that must be addressed. For the special features that demanded for cryogenic thermometer, such as non-contact, spatially resolved and high sensitivity at cryogenic temperature, soluble luminescence-dependent temperature sensor is a perfect candidate for cryogenic temperature detection.^{1,18,26}

Herein we report on a new approach to ratiometrically monitor cryogenic temperature based on dual emission from a small molecule 9-(9, 9-dimethyl-9H-fluoren-3yl)-14-phenyl-9, 14-dihydrodibenzo [a, c] phenazine (FIPAC, Fig. 1a) in 2-methyl-tetrahydrofuran (MeTHF) solution. Attributed to the temperature-dependent PL color rang from orange via magenta to blue upon cooling, the FIPAC system can be applied in visually detecting temperature. In addition, this temperature sensor system can also be used in high-resolution for the soluble character. Unlike the other previously reported dual emission molecules, dual emission of FIPAC is suggested to be attributed to the configuration transformation of two excited-states. This excited-state related character is temperature sensitive and leads to the temperature-dependent photoluminescence spectra, which sets the foundation for the application in ratiometric thermometer. This system can be applied in a wide temperature range from 138 K to 343 K with high sensitivity at low temperature, which is a candidate for cryogenic thermometer. We demonstrate that this FIPAC in MeTHF solution

^aBeijing National Laboratory for Molecular Sciences (BNLMS), Institute of Chemistry, Chinese Academy of Sciences, Beijing, 100190, China. E-mail: hongbing.fu@iccas.ac.cn, jinyao@iccas.ac.cn, yswu@iccas.ac.cn

^bUniversity of Chinese Academy of Sciences, Beijing, 100039, China

^cDepartment of Chemistry, Capital Normal University, Beijing, 100048, China

^dKey Laboratory for Advanced Materials and Institute of Fine Chemicals, East China University of Science & Technology, Shanghai, 200237, China. E-mail: tianhe@ecust.edu.cn

† Electronic Supplementary Information (ESI) available. See

DOI: 10.1039/x0xx00000x

cryogenic temperature sensor system with temperature-dependent dual emission from two excited-states is stable and reproducible.

Experimental

FIPAC was synthesized by a mean of copper-promoted coupling with N, N-diphenylphenanthrene-9, 10-diamine and 2-iodo-9, 9-dimethylfluorene as the starting materials.²⁷ For the high boiling point (353 K) and low melting point (137 K), the chemically stable liquid MeTHF was chosen as the medium for FIPAC to perform the temperature-dependent experiment.²⁸ The absorption spectra were recorded on SHIMADZU UV-3600. The room-temperature PL spectra were collected on Horiba Fluoromax-4NIR. The temperature-dependent PL spectra were collected on Edinburgh-FLSP920 and the temperature of sample was controlled by a cooling stage (HCS) from INSTEC. The emission spectra for every temperature range hadn't been collected until the temperature keep stable more than 5 minutes and the error for the measurement of the experiment temperature is not more than 0.3 K. The time-resolved photoluminescence (PL) decay transient spectra were executed by a streak camera system with a Ti: sapphire femtosecond laser system generating the pump pulses (370nm, 130 fs, 1 kHz). This system was also used to provide the pump pulses and the probe pulses for the femtosecond ultrafast transient absorption system.

The femtosecond ultrafast transient absorption system is based on the two probe beams system passing through two different parts of sample with one part of the sample is excited by the pump beam. Thus, we can calculate the absorbance difference for these two probe beams to obtain the absorption spectra of the excited-state. The laser pulses both for the pump and probe beams are generated by a Ti: sapphire femtosecond laser system. Detail for this system have been punished previously and only a brief description is given here.²⁹ The pump beams and probe beams are origin from the same laser pulse at 800 nm (120 fs, 1kHz) by using a 9:1 beam splitter. Then, the major component was sent to the optical parametric amplifier system to generate the pump beams while the remaining is focused into a 3-mm sapphire plate to generate the probe beams. Time delay between the pump beams and the probe beams is controlled by computer.

All theoretical work was executed by the Gaussian 09 program.³⁰ The ground state of FIPAC was calculated by the density functional theory (DFT) method and the excited states were calculated by the time-dependent density functional theory (TD-DFT) method. For all atoms, the geometries of molecule were optimized at the B3LYP/6-31+G* level in gas.

Results and discussion

Fig. 1a shows the absorption (black line) and PL spectra (blue line) of FIPAC in solution (MeTHF) at room temperature. The absorption maximum of FIPAC is located at ~360 nm. However, at a closer look of these room-temperature PL spectra, FIPAC exhibits unimaginable dual emission with an obviously abnormal Stokes-shifted emission band at ~595 nm and a weaker normal Stokes-shifted emission band at ~442 nm. The energy gap of ~0.72 eV between the two emission bands exceeds the span (~0.15 eV) of vibrational energy level, which indicates that these two emission bands come from two kinds of emission species. Meanwhile, ¹H NMR of FIPAC at

room temperature demonstrates there existing only one ground state (Fig. S1 top). In addition, the temperature-dependent ¹H NMR spectra for the aromatic part of FIPAC (range from 203 K to 303 K for every 20 K) (Fig. S1 bottom) and the temperature-dependent absorption spectra of FIPAC (vide infra) also preclude the possibility that the two emission species come from different ground states.

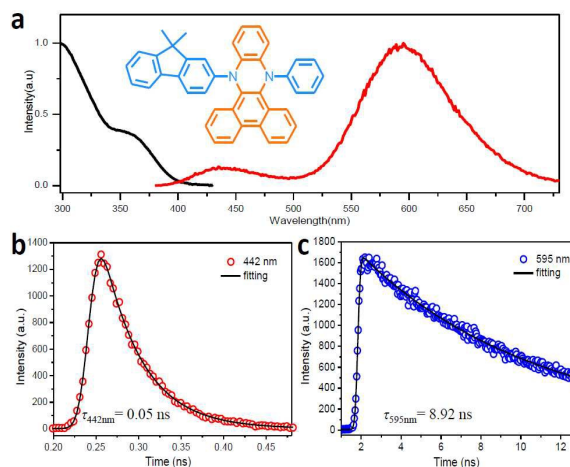


Fig. 1 (a) Absorption (298 K, black line), photoluminescence (PL) 298 K (red line) of FIPAC in MeTHF. The molecular structure of FIPAC is also presented. (b) Time-resolved PL decay transient of FIPAC in 442nm. (c) Time-resolved PL decay transient of FIPAC in 595nm. These points are data and the black solid line is the fitting line.

In order to investigate the dual emission mechanism of FIPAC, time-resolved PL decay transient of FIPAC was conducted with a streak camera system. Fig. 1b and 1c show the decay PL spectra located at the short-wavelength emission band (~442 nm) and the long-wavelength emission band (~595 nm), which indicates the intrinsic difference between these two emission bands. The short-wavelength emission follows a very fast decay with $\tau_{442\text{nm}} = 0.05$ ns. At the same time, lifetime of the long-wavelength emission reaches as long as 8.92 ns. The exceeding fast attenuation of the short-wavelength emission band presents an excited-state transformation mechanism from the excited-state corresponding to it.

To further verify the photogeneration and population of the involved excited states, we explored the ultrafast transient absorption spectra of FIPAC in MeTHF solution as shown in Fig. 2. Upon photoexcitation, FIPAC solution shows a decay on very short timescale absorption band at ~425 nm and ~500 nm. These absorption bands are attributed to one of the two excited-states absorption which is consistent with the 0.05 ns apparent from fig. 1b.³¹ By 181ps, however, the FIPAC solution is dominated by another excited-state absorption feature with a new peak at ~440 nm accompanied by a weaker peak at ~500 nm. The decay time of 6.92 ns for 440nm band and 6.73 ns for 500 nm band is similar to the long life time scale demonstrated in fig. 1c. Thus, the mechanism that one of these excited-states is rapidly formed upon photoexcitation and then fleetly decays in tens of picoseconds is confirmed. The decay of this excited-state either gives the short-wavelength emission or transforms to another excited-state, both of which result in the ultrafast decay of the excited-state which is corresponding to the short-wavelength emission. Because of the energy barrier existing in the excited-state configuration

transformations, controlling the ratio of these two excited-states through modulating temperature is operational feasibility.

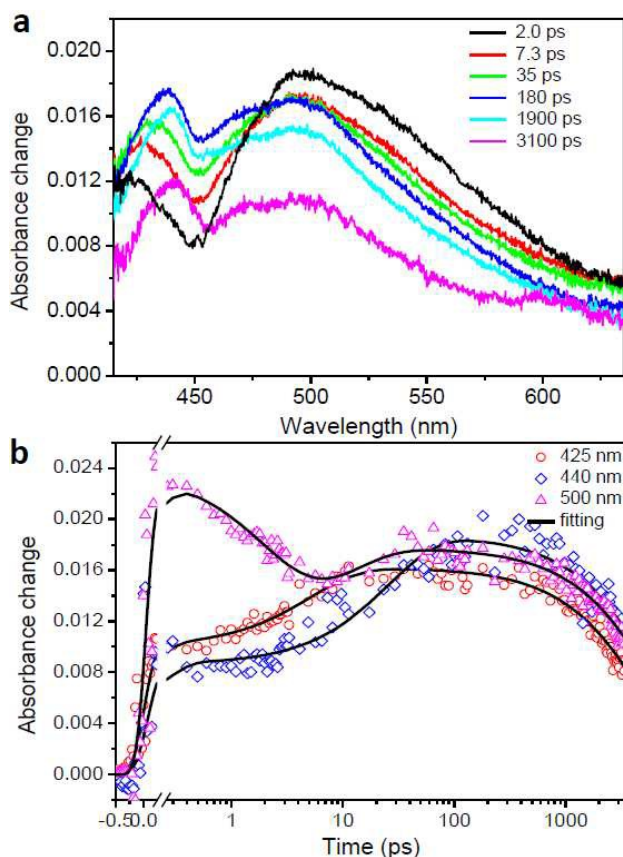
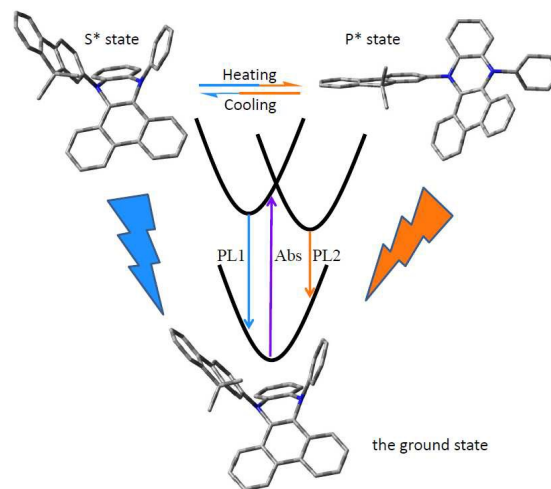


Fig. 2 (a) The femtosecond ultrafast transient absorption spectra of FIPAC in MeTHF solution. (b) The kinetics traces (colored points) and fitting lines (black solid line) taken from the short-wavelength emission excited-state (~ 425 nm and ~ 500 nm) and the long-wavelength emission excited-state (~ 440 nm and ~ 500 nm) absorption features with major overlap with each other for FIPAC in MeTHF.

According to the recently reported work,^{27,32} FIPAC exhibits a saddle-like structure in the ground state, which distorted at the two N atoms line of the dihydrodibenzo[a,c]phenazine subject for the steric effect of the two N,N'-disubstitutes and the phenanthrene ring. Computational study at B3LYP/6-31+G* level gives the structures of these two excited-states, which exhibit completely different configurations (Scheme 1): the saddle-like excited-state is referred as the S* state and the planner-like excited-state is referred as the P* state. Meanwhile, the initial frank-condon excited-state is short as the F* state. According to the calculated optical features as shown in Table 1, the S* state should be corresponding to the short-wavelength emission and the P* state should be corresponding to the long-wavelength emission. Thus, an outline of the excited-state configuration transformations mechanism for the dual-emission of FIPAC is developed. Upon photoexcitation, the S* state is rapidly formed and then quickly decays in two routes. The first is to give the short-wavelength emission and the second is to transform to the P* state after overcoming some energy barriers (referred as ΔE) accompanied by

the excited-state configuration changed. Then, the P* state gives the long-wavelength emission. The calculated relative energy as shown in Table 1 shows that the P* state is 0.1168 eV more stable than the S* state, which gives enough driving force for the configuration transformation. Importantly, this excited-state configuration transformations process is energy controlled, which can be regulated by temperature. Therefore, with more or fewer excited-states transformation upon heating or cooling, ratio of the dual emission intensity differs at different temperature, which can be used as a parameter to describe temperature. In addition, for the much stronger luminescence intensity at cryogenic temperature (Fig. S2 and Table S1), the FIPAC system will undoubtedly exhibits a good performance for the cryogenic temperature detection.



Scheme 1 Excited states configuration transform with temperature ranges. Atom color: C in gray, N in blue.

In terms of cryogenic temperature and solid phase may prevent the excited-state configuration transforming, we performed the cryogenic PL at 77 K (red line in Fig. 3a) and solid PL spectra at room temperature (blue line in Fig. 3a). Cryogenic PL at 77 K reveals only one emission band at ~ 405 nm which is supposed to be the consequence of the slower vibration relaxation and the almost impossible excited-state configuration transformations by the lattice

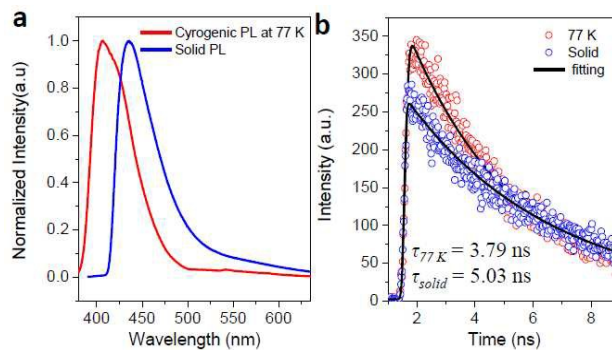


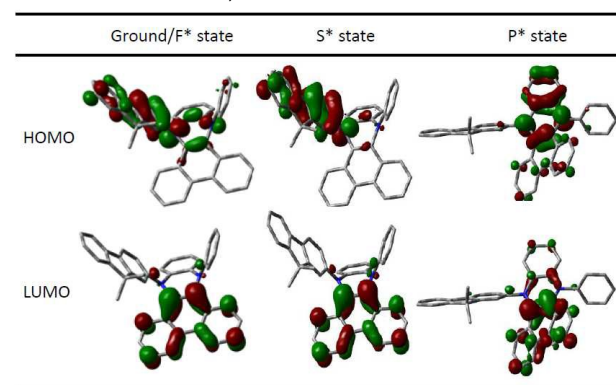
Fig. 3 (a) PL at 77 K (red line) for FIPAC in MeTHF solution and solid PL for FIPAC at room temperature. (b) Time-resolved PL decay transient of FIPAC in MeTHF at 77 K (red cycles) and in solid phase at room temperature (blue cycles). The points are data and the black solid line is the fitting line.

Table 1. The experimental and calculated results of properties for FIPAC.^a

state	Optical features			Stokes shift		τ_f (ns) ^d	Calculated relative energy (eV) ^e	calculated dipole moment (Debye)
	λ_{exp} (nm) ^b	λ_{cal} (nm) ^b	f ^c	Exp (cm ⁻¹)	Cal (cm ⁻¹)			
ground /F*	361	408	0.1005	-	-	-	0.4928	1.7092
S*	435	537.8	0.0445	4170	5920	0.046	0.1168	3.3535
P*	595	728.6	0.0558	10890	10790	8.92	0	0.7975

^aAll experimental data were performed in MeTHF solution at room temperature. ^b λ stands for the lowest-lying absorption or emission peak wavelength. ^cf stands for the calculated oscillator strengths. ^d τ_f stands for the population decay time. ^eCalculated relative energy is the relative energy with the P* state as the referenced state.

-e constraint. In comparison, solid FL of FIPAC also shows a single but red-shifted band at ~435 nm. This emission band, from the point of the above mechanism, should be ascribed to the immutable configuration accompanied with vibration relaxation in the solid phase, which is consistent with the short-wavelength emission in solution. As a result, the cryogenic temperature and solid phase strongly hinder the excited-state configuration transforming. Based on this, we performed the time-resolved PL decay transient of FIPAC in MeTHF at 77 K (red cycles) and in solid phase at room temperature (blue cycles). The fact that lifetime of the short-emission band at 77 K and in solid phase at room temperature extending to 3.79 ns and 5.03 ns confirms the above mechanism further. With little competition from configuration transforming to the P* state, decay of the S* state which is corresponding to the short-wavelength emission ranges from tens of picoseconds to several nanoseconds.

Table 2. HOMO and LUMO of the ground state and the relaxed structure in the F* state, S* state and P* state.

In order to further confirm the above computation work, results of computation work were introduced to interpret the solvent effect experiment (Fig. S3). The absorption spectra demonstrate a non-solution sensitive feature without absorption band shift. In contrast to the neglectful shift in the long-wavelength emission band, the short-wavelength emission band reveals a not so small red-shift ranging from cyclohexane (CYH), MeTHF and acetonitrile (MeCN). We attribute this phenomenon to be the different charge transfer characters and dipole moments between the S* state and the P* state. Table 2 exhibits the frontier molecular orbitals for these three FIPAC states, which shows that the charge transfer character of the F* state and the S* state is more obvious than that

of the P* state. In addition, computational work also gives a huge difference among the dipole moments of the ground state/F* state, S* state and P* state (1.7092 Debye, 3.3535 Debye and 0.7975 Debye, respectively) (Table 1). The large dipole moment and obvious charge transfer character for the S* state results in the red-shift of the short-wavelength emission in the solvent effect experiment. Therefore, the computational result is perfectly consistent with the experimental result, which demonstrates that our excited-state configuration mechanism for the dual-emission of FIPAC is logical.

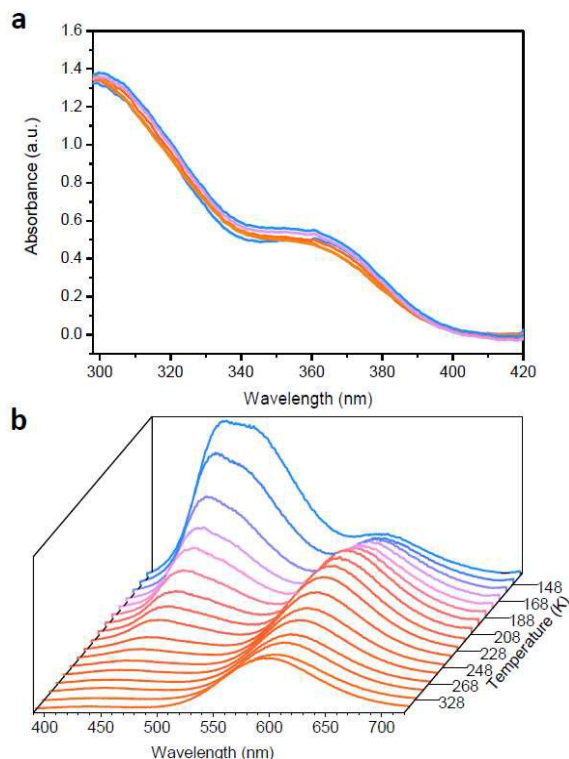


Fig. 4 (a) Absorption of FIPAC in MeTHF between 138K and 343K. (b) The emission spectra of FIPAC in MeTHF between 138K and 343K (excitation wavelength 370nm). Every 20 K for spectra from 138 K to 268 K and after 268 K the three spectra are at 298 K, 328 K and 343 K.

Fig. 4 demonstrates the temperature-dependent absorption and emission spectra of FIPAC from 138 K to 343K. The non-

temperature-sensitive of the absorption bands precludes the possibility of the ground state configuration changes with temperature range,⁹ which is further confirmed by the temperature-dependent ¹H NMR spectra (from 203 K to 303 K for every 20 K) (Fig. S1). In contrast, PL of FIPAC expresses a completely distinct temperature-related property. At room temperature, the long-wavelength emission contributes the main emission band. Meanwhile, the short-wavelength emission becomes the dominated luminescence without any significant shifts for the long-wavelength emission at low temperature. Thus, the temperature-dependent PL emission is attributed to the variation of excited-state configuration at different temperature.²⁰ Therefore, we can conclude that the dual emission of this soluble FIPAC system derived from two kinds of excited-states. The equilibrium between these two excited-states will be controlled by temperature and the PL spectrum will be a Boltzmann-weighted sum of contributions from these two excited-states. As a result, PL of this FIPAC system will reflect the environment temperature. On the other words, the temperature-dependent PL spectra raise the possibility to ratiometrically monitor temperature.

The temperature-dependent PL spectra also reveal the quantitative relationship between the PL of FIPAC and temperature. Fig. 5a depicts the ratio of the integrated area of short-wavelength emission band to the integrated area of long-wavelength emission band (referred as A_s/A_l), which as a function of temperature (from 138 K to 343 K). This single-exponential relationship can be fitted as $A_s/A_l = 0.05149 + 1652.3173 \exp(-T/23.40204)$ with correlation coefficient 0.9956, where T is the kelvin temperature. As illustrated above, this temperature-dependent feature for A_s/A_l of FIPAC is ascribed to the temperature controlled excited-state configuration transformations, which gives different excited-states distributions with the range of temperature. To further illustrate this temperature-related process, relationship between the ratio A_s/A_l and $1/T$ is shown in Fig. 5a inset. As expected, it can also be fitted as a single-exponential function with correlation coefficient 0.9910: $A_s/A_l = -0.0947 + 0.0044 \exp(1/0.00104 T)$, where T is the kelvin temperature. Since the intensity of emission band is proportional to the number of the corresponding excited states, it is reasonable to apply A_s/A_l in the following equation:

$$\frac{A_s}{A_l} \propto \frac{\alpha_s \cdot N_{S^*}}{\alpha_p \cdot N_{P^*}} = \frac{\alpha_s}{\alpha_p} \cdot \frac{N \cdot N_{S^*} \cdot e^{-\frac{\Delta E}{kT}}}{N \cdot e^{-\frac{\Delta E}{kT}}} = \frac{\alpha_s}{\alpha_p} \cdot \frac{1 - e^{-\frac{\Delta E}{kT}}}{e^{-\frac{\Delta E}{kT}}} = \frac{\alpha_s}{\alpha_p} \cdot e^{\frac{\Delta E}{kT}} - \frac{\alpha_s}{\alpha_p}$$

Where A_s and A_l are the integrated area of short-wavelength band emission and long-wavelength band emission; N , N_{S^*} and N_{P^*} are the number of all the excited states, the S^* states and the P^* states, respectively; α_s , α_p are the radiative transition efficiency for the S^* state and the P^* state, respectively; ΔE is the energy barrier of excited state configuration transformations from the S^* state to the P^* state.; T is the kelvin temperature and k is the Boltzmann constant.^{33,34}

Hence, the energy barrier was calculated to be $\Delta E = 0.08279$ eV (see electronic supplementary information). The calculated result $\Delta E = 0.08673$ eV in He Tian and co-workers' work is close to our results.²⁷ This low energy barrier lays the foundation of applying this system in cryogenic temperature detection field for which the excited-state configuration transformations could occur at very low temperature. As a consequence, we have given a consummate interpretation for the configuration transformation of excited states

both from experiment and theory derivation, which strongly supports that the ratio A_s/A_l for this system is a good parameter to describe temperature.

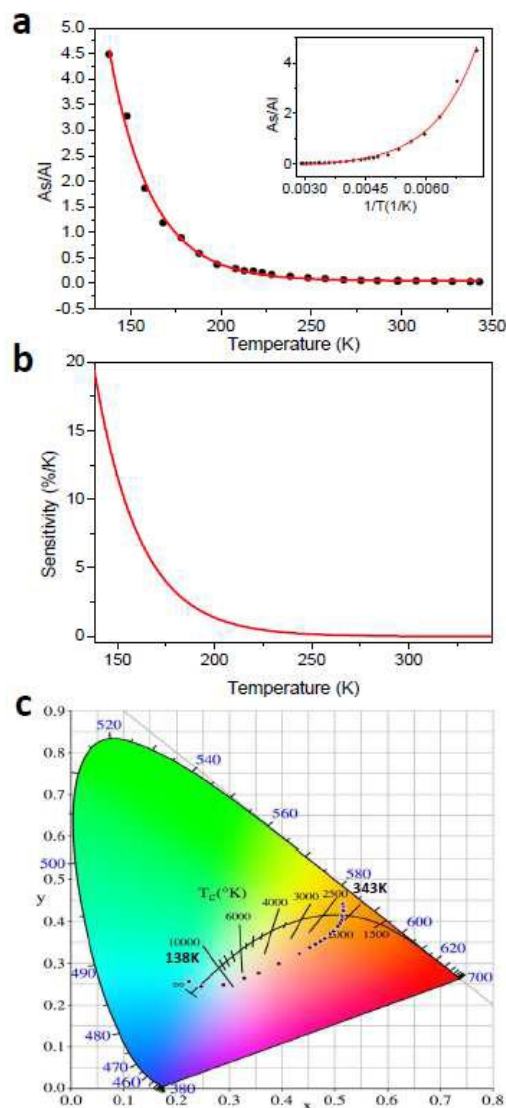


Fig. 5 (a) Plots of A_s/A_l vs. temperature changes. inset: Plots of A_s/A_l vs. $1/T$ changes. The points are data and the line is a polynomial fit. (b) Temperature dependence of the sensitivity according to the equation $S(T) = |\partial(A_s/A_l)/\partial T|$. (c) CIE chromaticity diagram showing the luminescence colors of FIPAC in MeTHF at different temperature.

More significantly, the sensitivity in the temperature range is also calculated according to the equation: $S(T) = |\partial(A_s/A_l)/\partial T|$ (Fig. 5b).^{1,26} It can be inferred that FIPAC possess a higher sensitivity at lower temperature and the sensitivity reaches as high as 19.4 % per K at 138 K. This high sensitivity results from the low rate of excited-state configuration transformations which is due to both the low energy level for the population of the S^* state and the harder configuration changes at low temperature. In addition, the quantum yields of FIPAC reaches more than 17.7% compared with the value of 5.0% at room temperature (Table S1), which

demonstrates that the FIPAC system is a good candidate for the detection of cryogenic temperature.

Although the thermosensitive ratio of dual emission intensity is adequately suitable for the detection of cryogenic temperature, there exists the difficulty in the separation of the two emission bands. For the more convenient application of this soluble cryogenic temperature sensor system, the temperature-dependent spectra were transformed to the Commission Internationale de L'Eclairage (CIE) 1931 coordinates in Fig. 5c. The color shifts from orange via magenta to blue upon cooling is easily observable both for naked-eye and camera. This temperature-dependent emission color ranging is due to the variation of the population of these two excited-states. The pure S^* state gives a deep blue emission and the pure P^* state exhibits an orange emission. As a consequence, different distributions for these two excited-state will demonstrate diverse emission color. Thus, color of the FIPAC's emission can be taken as a method for the detection of temperature. This scope of temperature ranging from 138 K to 343 K is competent for the detection of temperature in expedition of the dipole, space exploration, material research and other filed that need accurate cryogenic temperature detection.

To further apply the FIPAC system in practical, we filled a quart tube with FIPAC in MeTHF solution to demonstrate the gradient PL of the FIPAC system at different temperature as shown in Fig. 6. The top of the quart tube was slight heated and the bottom was cooled. Thus, a continuously color changed from orange via magenta to blue upon cooling is observable for naked-eye. We can also note that the PL color of this system changes sensitively at cryogenic temperature from 138 K to 218 K, which is consistent with the result of Fig. 5b. Therefore, temperature of environment can either be directly estimated from the PL color of the FIPAC system by naked-eye or be accurately measured by comparing the PL color with the temperature-dependent CIE chromaticity diagram as shown in Fig. 5c. This visible method for the measurement of temperature offers a convenient way to detect temperature distribution.

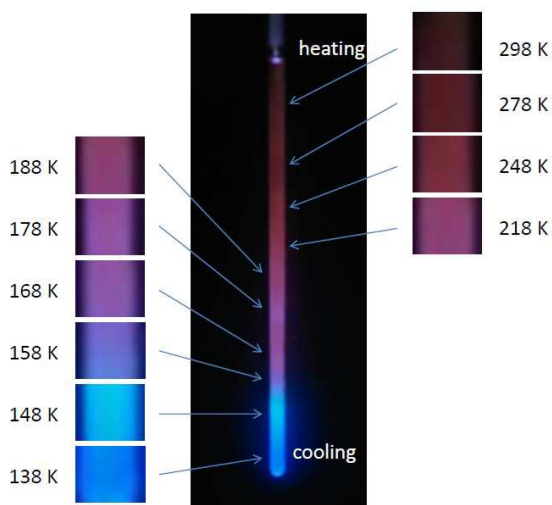


Fig. 6 Photographs represent of PL color for the FIPAC system at different temperature and the gradient PL of the FIPAC system in a quart tube.

Besides the application in temperature detection, the FIPAC system can be used in the detection of viscosity, too.²⁷ High viscosity will prevent the excited-state configuration transformations, which will lead to the viscosity-dependent PL. Thus, the FIPAC system can be a good candidate as fluorescence dye in some cases such as industrial painting applications.⁹ However, in contrast to the energy control in temperature-dependent PL, influence of viscosity on PL is time-dependent. Given enough time, the S^* state will transform to the P^* state and the PL will be independent of viscosity but be temperature-dependent.²⁷ Therefore, further experiments are needed to apply this FIPAC system in the detection of viscosity.

Conclusions

In summary, we have demonstrated a soluble cryogenic temperature sensor system based on the small molecule FIPAC in MeTHF solution. This system is appropriate for broad temperature range from 138 K to 343 K with luminescence color varying from blue via magenta to orange. Unlike the other dual emission molecules, dual emission of FIPAC is suggested to be attributed to the configuration transformation of excited-states. Time-resolved PL transient of FIPAC shows that the lifetime of the two excited-states differs at one order of magnitude and the transformation progress can be demonstrated in the femtosecond ultrafast transient absorption spectra. Lifetime of FIPAC in solid phase and at 77K demonstrates that the excited-state configuration transformations contributes to the main decay of the S^* state. Computational work and theory derivation also gives supports for the experimental data. As a result, excited-state configuration transformation triggered temperature-dependent PL spectra set the foundation for the application of this system in the thermometer filed. By using this temperature detection system, the ratio A_s/A_l or the PL color can be correlated to the temperature values. This system also demonstrates extremely high sensitivity at low temperature with the value of 19.4 % per K at 138 K. Therefore, a high sensitivity, accurate, observable, and convenient cryogenic thermometer system as titled is built.

Acknowledgements

This work was supported by the National Natural Science Foundation of China (Nos. 91222203, 21273251, 91333111, 21190034, 21221002), project of State Key Laboratory on Integrated Optoelectronics of Jilin University (IOSKL2014KF19), project of Construction of Innovative Teams and Teacher Career Development for Universities and Colleges Under Beijing Municipality (IDHT20140512), the National Basic Research Program of China (973) 2011CB808402, 2013CB933500, and the Chinese Academy of Sciences.

References

- 1 X. D. Wang, O. S. Wolfbeis and R. J. Meier, *Chem. Soc. Rev.*, 2013, **42**, 7834.
- 2 P. R. N. Childs, J. R. Greenwood and C. A. Long, *Rev. Sci. Instrum.*, 2000, **71**, 2959.

- 3 L. P. Goss, A. A. Smith and M. E. Post, *Rev. Sci. Instrum.*, 1989, **60**, 3702.
- 4 C. D. Brites, P. P. Lima, N. J. Silva, A. Millan, V. S. Amaral, F. Palacio and L. D. Carlos, *Nanoscale*, 2012, **4**, 4799.
- 5 D. Jaque and F. Vetrone, *Nanoscale*, 2012, **4**, 4301.
- 6 M. D. Chambers and D. R. Clarke, *Annu. Rev. Mater. Res.*, 2009, **39**, 325.
- 7 A. J. B. Sami D. Alaruri, Mark A. Thomas and Jeff A. Miller, *IEEE T. Instrum. Meas.*, 1993, **42**, 735.
- 8 M. Megahed, *Appl. Opt.*, 1993, **32**, 4790.
- 9 J. Feng, K. Tian, D. Hu, S. Wang, S. Li, Y. Zeng, Y. Li and G. Yang, *Angew. Chem. Int. Ed.*, 2011, **50**, 8072.
- 10 P. Low, B. Kim, N. Takama and C. Bergaud, *Small*, 2008, **4**, 908.
- 11 S. M. Borisov, A. S. Vasylevska, C. Krause and O. S. Wolfbeis, *Adv. Funct. Mater.*, 2006, **16**, 1536.
- 12 X.-c. Shan, F.-l. Jiang, D.-q. Yuan, H.-b. Zhang, M.-y. Wu, L. Chen, J. Wei, S.-q. Zhang, J. Pan and M.-c. Hong, *Chem. Sci.*, 2013, **4**, 1484.
- 13 L. Jethi, M. M. Krause and P. Kambhampati, *J. Phys. Chem. Lett.*, 2015, **6**, 718.
- 14 E. M. Graham, K. Iwai, S. Uchiyama, A. P. de Silva, S. W. Magennis and A. C. Jones, *Lab Chip*, 2010, **10**, 1267-1273.
- 15 G. Baffou, C. Girard and R. Quidant, *Phys. Rev. Lett.*, 2010, **104**, 136085.
- 16 X. Rao, T. Song, J. Gao, Y. Cui, Y. Yang, C. Wu, B. Chen and G. Qian, *J. Am. Chem. Soc.*, 2013, **135**, 15559.
- 17 M. Mitsuishi, S. Kikuchi, T. Miyashita and Y. Amao, *J. Mater. Chem.*, 2003, **13**, 2875.
- 18 E. J. McLaurin, L. R. Bradshaw and D. R. Gamelin, *Chem. Mater.*, 2013, **25**, 1283.
- 19 C.-K. L. Jye-Shane Yang, Anand M. Lahoti, Chung-Kai Tseng, Yi-Hung Liu, Gene-Hsiang Lee, and Shie-Ming Peng, *J. Phys. Chem. A*, 2009, **113**, 4868.
- 20 C. C.-G. a. W. Rettig, *J. Phys. Chem. A*, 1998, **102**, 7754.
- 21 S. K. Mellerup and S. Wang, *Organometallics*, 2014, **33**, 5483.
- 22 K. Wang, J. Qian, D. Jiang, Z. Yang, X. Du and K. Wang, *Biosens. Bioelectro.*, 2014, **65C**, 83.
- 23 V. A. Vlaskin, N. Janssen, J. van Rijssel, R. Beaulac and D. R. Gamelin, *Nano Lett*, 2010, **10**, 3670.
- 24 C. Y. Chen and C. T. Chen, *Chem. Commun. (Camb)*, 2011, **47**, 994.
- 25 C. d. Tard, S. Perruchas, S. b. Maron, X. F. Le Goff, F. o. Guillen, A. Garcia, J. Vigneron, A. Etcheberry, T. Gacoin and J.-P. Boilot, *Chem. Mater.*, 2008, **20**, 7010.
- 26 Y. Guo, S. Gu, X. Feng, J. Wang, H. Li, T. Han, Y. Dong, X. Jiang, T. D. James and B. Wang, *Chem. Sci.*, 2014, **5**, 4388.
- 27 Z. Zhang, Y. S. Wu, K. C. Tang, C. L. Chen, J. W. Ho, J. Su, H. Tian and P. T. Chou, *J. Am. Chem. Soc.*, 2015, **137**, 8509.
- 28 V. Pace, P. Hoyos, L. Castoldi, P. Dominguez de Maria and A. R. Alcantara, *ChemSusChem*, 2012, **5**, 1369.
- 29 Y. Wu, K. Liu, H. Liu, Y. Zhang, H. Zhang, J. Yao and H. Fu, *J. Phys. Chem. Lett.*, 2014, **5**, 3451.
- 30 G. W. T. M. J. Frisch, H. B. Schlegel, G. E. Scuseria, M. A. Robb, J. R. Cheeseman, G. Scalmani, V. Barone, B. Mennucci, G. A. Petersson, H. Nakatsuji, M. Caricato, X. Li, H. P. Hratchian, A. F. Izmaylov, J. Bloino, G. Zheng, J. L. Sonnenberg, M. Hada, M. Ehara, K. Toyota, R. Fukuda, J. Hasegawa, M. Ishida, T. Nakajima, Y. Honda, O. Kitao, H. Nakai, T. Vreven, J. A. Montgomery, Jr., J. E. Peralta, F. Ogliaro, M. Bearpark, J. J. Heyd, E. Brothers, K. N. Kudin, V. N. Staroverov, R. Kobayashi, J. Normand, K. Raghavachari, A. Rendell, J. C. Burant, S. S. Iyengar, J. Tomasi, M. Cossi, N. Rega, J. M. Millam, M. Klene, J. E. Knox, J. B. Cross, V. Bakken, C. Adamo, J. Jaramillo, R. Gomperts, R. E. Stratmann, O. Yazyev, A. J. Austin, R. Cammi, C. Pomelli, J. W. Ochterski, R. L. Martin, K. Morokuma, V. G. Zakrzewski, G. A. Voth, P. Salvador, J. J. Dannenberg, S. Dapprich, A. D. Daniels, O. Farkas, J. B. Foresman, J. V. Ortiz, J. Cioslowski, and D. J. Fox, Gaussian, Inc., Wallingford CT,, Gaussian 09, Revision **A.02**, 2009.
- 31 B. J. Walker, A. J. Musser, D. Beljonne and R. H. Friend, *Nat. Chem.*, 2013, **5**, 1019.
- 32 W. Huang, L. Sun, Z. Zheng, J. Su and H. Tian, *Chem. Commun.*, 2015, **51**, 4462.
- 33 R. Hasegawa, I. Sakata, H. Yanagihara, B. Johansson, A. Omrane and M. Aldén, *Appl. Phys. B*, 2007, **88**, 291.
- 34 J. Mooney and P. Kambhampati, *J. Phys. Chem. Lett.*, 2013, **4**, 3316.

Paper

PCCP

SYNOPSIS TOC

